Open access • Journal Article • DOI:10.1149/1.2220978

Galvanostatic Pulse and Pulse Reverse Plating of Nickel-Iron Alloys from Electrolytes Containing Organic Compounds on a Rotating Disk Electrode — Source link

Branko N. Popov, Ken-Ming Yin, Ralph E. White

Institutions: University of South Carolina

Published on: 01 May 1993 - Journal of The Electrochemical Society (The Electrochemical Society)

Topics: Rotating disk electrode, Linear sweep voltammetry, Plating, Voltammetry and Electroplating

1993

Galvanostatic Pulse and Pulse Reverse Plating of Nickel-Iron Alloys from Electrolytes Containing Organic Compounds on a Rotating Disk Electrode

Branko N. Popov
University of South Carolina - Columbia, popov@engr.sc.edu

Ken-Ming Yin
University of South Carolina - Columbia

Ralph E. White
University of South Carolina - Columbia, white@cec.sc.edu

Publication Info

Journal of the Electrochemical Society, 1993, pages 1321-1330.

Publisher's link: http://dx.doi.org/10.1149/1.2220978
DOI: 10.1149/1.2220978

Manuscript submitted June 24, 1992; revised manuscript received Jan. 4, 1993.

L'École Nationale Supérieure d'Electrochimie et d'Electrometallurgie de Grenoble assisted in meeting the publication costs of this article.

REFERENCES

1. R. Baboian, D. L. Hill, and R. A. Bailey, *This Journal,* **112,** 1221 (1965).
2. T. Sakura and T. Kirihara, *Denki Kagaku,* **36,** 320 (1968).
3. T. Sakura and T. Kirihara, *ibid.,* **37,** 107 (1969).
4. C. G. Sen, M. Okida, and T. Oki, *J. Appl. Electrochem.,* **20,** 77 (1990).
5. S. A. Kuznetsov, P. T. Stangrit, and S. V. Kuznetsova, *Elektrokhimiya,* **26,** 63 (1990).
6. S. A. Kuznetsov and P. T. Stangrit, Paper presented at the ISE Meeting, Prague, 1990.
7. T. A. Puzanova, M. V. Smirnov, and N. A. Loginov, *Elektrokhimiya,* **17,** 369 (1971).
8. T. A. Puzanova and M. V. Smirnov, *ibid.,* **16,** 1563 (1980).
9. P. Moinard, Ph.D. Thesis, INP, Grenoble (1983).
10. J. P. Garnier, Ph.D. Thesis, INP, Grenoble (1985).
11. G. J. Kipouros and S. N. Flengas, *Can. J. Chem.,* **61,** 2183 (1983).
12. J. Bouteillon and A. Marguier, *Surf. Technol.,* **22,** 205 (1984).
13. M. Taoumi, J. Bouteillon, and M. J. Barbier, *Electrochim. Acta,* **31,** 837 (1986).
14. F. A. Shunk, *Constitution of Binary Alloys,* Second Supplement, McGraw-Hill, Inc., New York (1969).
15. *The Handbook of Binary Phase Digrams,* General Electric Company, Business Growth Services, Schenectady, NY (1976).
16. J. M. Savéant and D. Tessier, *J. Electroanal. Chem.,* **65,** 57 (1975).
17. D. Renaud, Ph.D. Thesis, INP, Grenoble (1985).
18. M. Goto and K. B. Oldham, *Anal. Chem.,* **45,** 2043 (1973).
19. H. Matsuda and Y. Ayabe, *Z. Elektrochem.,* **59,** 494 (1955).
20. M. Taoumi, Ph.D. Thesis, INP, Grenoble (1986).
21. H. W. Vandenborn and D. H. Evans, *Anal. Chem.,* **46,** 643 (1974).
22. M. A. Bredig, J. W. Johnson, and W. T. Smith, *J. Am. Chem. Soc.,* **77,** 307 (1955).
23. A. Robin, Ph.D. Thesis, INP, Grenoble (1987).
24. G. J. Janz and N. P. Bansal, *J. Phys. Chem. Ref. Data,* **11** (1982).

Galvanostatic Pulse and Pulse Reverse Plating of Nickel-Iron Alloys from Electrolytes Containing Organic Compounds on a Rotating Disk Electrode

B. N. Popov,* Ken-Ming Yin,[a] and R. E. White*

Department of Chemical Engineering, University of South Carolina, Columbia, South Carolina 29208

ABSTRACT

Linear sweep voltammetry, galvanostatic pulse, and pulse reverse techniques were used to study the plating of nickel-iron alloys in the presence of organic additives. The effects of pulse current densities, i_p, reverse current densities, i_r, rotation speed of disk electrode, and the presence of organic additives on deposition of nickel-iron alloys are evaluated. The observed phenomena can be explained by the concentration depletion of reactants (or products), and the surface coverage of the additives on the electrode. A new formulation of the plating bath is defined.

Electrodeposition of nickel-iron alloys is classified as anomalous codeposition because the discharge rate of the more noble component Ni is inhibited, causing the appearance of the less noble metal Fe at a higher ratio in the deposit than that in the electrolyte.[1-6] Explanations of the deposition mechanism are diverse. According to Dahms,[1,2] anomalous codeposition appears closely related to the local pH rise at the interface due to the parallel parasitic hydrogen evolution. According to this theory, the preferential precipitation of iron hydroxide compared to nickel hydroxide causes the inhibition of nickel deposition. Iron discharges according to these authors through the iron hydroxide film.

Dahms and Croll's mechanism was revised by Romankiw,[7] who suggested that a trace amount of Fe^{3+} in the solution causes precipitation of $Fe(OH)_3$, and that such a film accounts for the selective discharge. Other researchers[8,9] attributed the underpotential deposition to the appearance of an iron dominant intermetallic compound. Recently, a steady-state Fe-Ni deposition model in which the anomalous codeposition was explained by the discharge rates of intermediate species $Fe(OH)^+$ and $Ni(OH)^+$ was proposed by Hessami and Tobias.[10] Pulse and pulse reverse plating reduced the Fe content, *i.e.,* reduced the anomalous behavior.[11]

Since both hydrogen evolution and iron deposition in the plating of Fe-Ni alloys are mass transport control,[1-4] the presence of organic additives (saccharin and butenediol) in the electrolyte may suppress the hydrogen evolution by absorbing on the surface of the substrate and play a significant role in Fe-Ni deposition. Also, saccharin may relieve the stress of the deposited alloy. Butenediol improves the brightness of the deposit. In the preliminary experiments in the presence of this additive a brilliant leveling Fe-Ni plate was obtained. In this work linear sweep voltammetry was used to characterize electrochemically formed Fe-Ni alloys. The object of this work is also to deposit Fe-Ni films using galvanostatic pulse and pulse reverse plating from sulfate baths in the presence and absence of organic additives for different agitation conditions.

* Electrochemical Society Active Member.

[a] Present address: Chemical Engineering Department, Yuan-Ze Institute of Technology, Neili, Taoyuan, Taiwan 320, China.

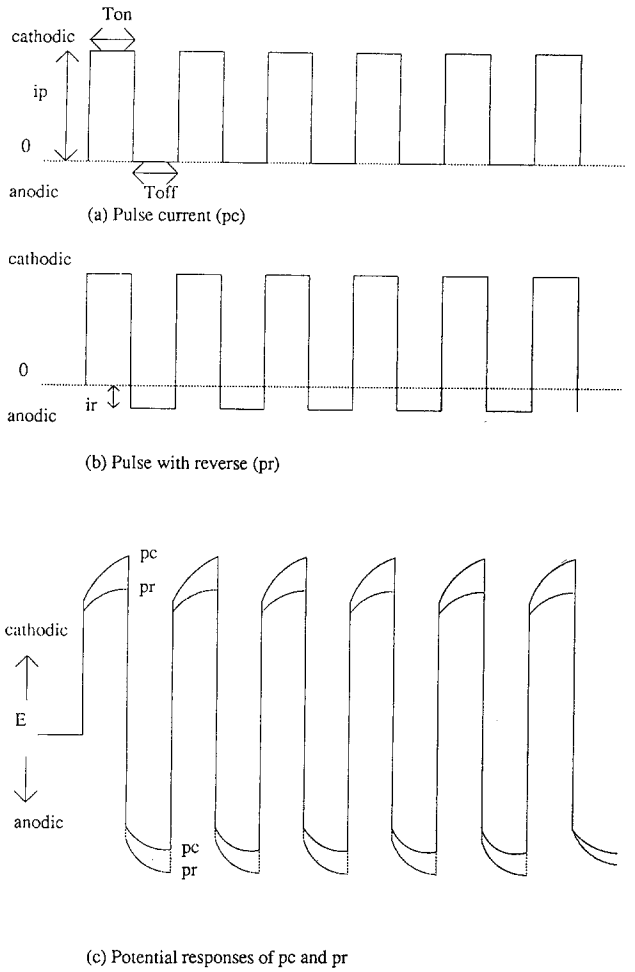

Fig. 1. Schematic diagrams of (a) pulse current (pc) waves; (b) pulse with reverse (pr); and (c) potential responses of pc and pr.

Experimental

Two types of plating solutions were used: a plain plating solution contained nickel sulfate (0.5*M*), iron sulfate (0.05*M*), and sodium sulfate (0.5*M*). The second plating solution contained ingredients from the plain bath + boric acid (0.5*M*), sodium saccharin (0.0166*M*), and 2 butene 1-4 diol (0.116*M*). The bath pHs were adjusted to 3 by using 20% H_2SO_4 and experiments were carried out at room temperature for all baths. Copper disks with exposed area of 0.458 cm^2 were used as the working electrodes; the anode used was a large platinum gauze and a SCE served as the reference electrode. Before each experiment, the copper disk was polished by using 400, 600 grit sand papers and then by using 0.3, 0.05 μm aluminum powder (Banner Scientific). The electrode was then cleaned with acetone and 10% H_2SO_4 solution before plating.

A schematic of the pulse wave form and the associated potential responses are shown in Fig. 1. Pulse current was applied by the potentiostatic/galvanostat Model 273 (PAR). The applied pulse current and associated potential responses were monitored by an oscilloscope (Textronix 2430A digital oscilloscope). The peak cathodic potential (at the end of T_{on}) and the peak anodic potential (at the end of T_{off}) were recorded as E_p and E_r, respectively. From the preliminary experiments we found that the current deposition efficiency is not a function of the pulse lengths. The pulse period (T_{on}) and relaxation period (T_{off}) were set at 100 ms each, and i_p was varied. The duty cycle of 0.5 was convenient in the experiments where i_p varies. For the pr mode $i_r = -0.2i_p$ for all operating conditions. The composition of the deposited alloys were measured by electron dispersion spectroscopy (EDS) and the surface morphologies were studied by SEM (JEOL JSM-35 CF scanning electron microscope in conjunction with Northern TN-200 x-ray analysis system).

Results and Discussion

Linear sweep voltammetry (LSV).—LSV was used as *in situ* technique to study single metal and alloy electrodeposition and dissolution. LSV was applied to dissolve anodically the alloy by using a fixed and rotating disk electrode.

Anomalous codeposition of Fe-Ni alloy appears to be closely related to the effect of hydrogen evolution and a local pH rise at the surface. Our study has included investigations of some aspects of hydrogen evolution. Specifically, the effectiveness of different concentrations of organic additive such as saccharin in suppressing the hydrogen evolution reaction was studied. Pt rotating disk electrodes were used as working electrodes. The hydrogen evolution reaction was investigated in 0.5*M* Na_2SO_4 solutions, containing neither Ni(II) nor Fe(II) ions. This study was conducted to determine the optimum concentration of saccharin which would be used in the electrodeposition process. LSV of a Pt rotating disk electrode in 0.5*M* Na_2SO_4 obtained at sweep rate of v = 30 mV/s and pH 3 is shown in Fig. 2. As seen in Fig. 2, (curves 2 and 3) the hydrogen evolution peak decreases with an increase in the concentration of saccharin till a concentration of the additive reaches 0.016*M* in the electrolyte. The hydrogen evolution reaction is lowest when the concentration of the additive is sufficient to exceed the minimum fractional coverage of the surface. Figure 3 shows the limiting hydrogen current obtained in 0.5*M* Na_2SO_4 solution in the presence of different concentrations of saccharine. As seen in Fig. 3 a cathodic shift of the water reduction overpotential (200 mV) and a decrease of the hydrogen limiting current was observed.

Boric acid is used extensively in plating systems as a buffer to lessen the pH rise at the surface. Tilak *et al.*[12] attribute the greater buffer capacity in nickel-containing solutions to a complexation of Ni(II) with boric acid. The effect of saccharin and boric acid on hydrogen evolution is shown in Fig. 4. The curves were obtained using a scan rate

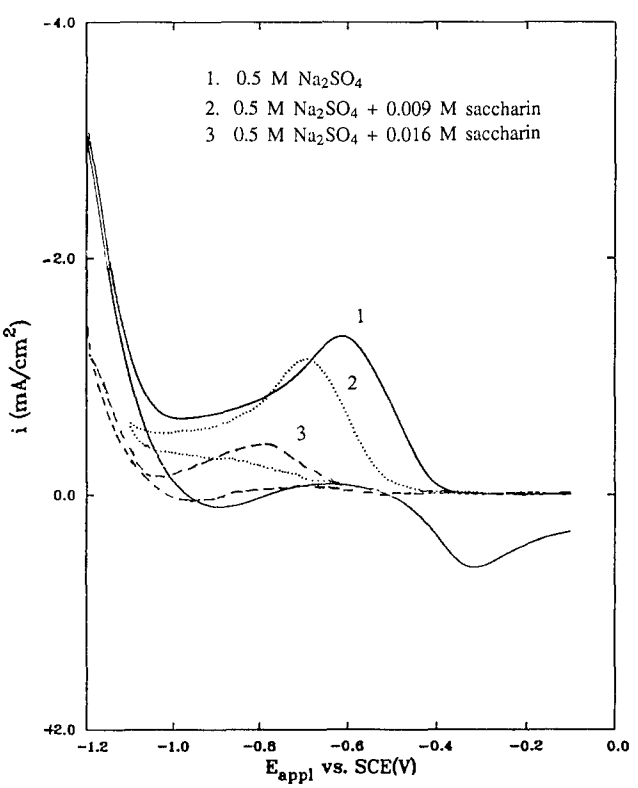

Fig. 2. Effect of saccharin on hydrogen evolution. Linear sweep voltammetry of Pt rotating disk electrode in 0.5*M* Na_2SO_4, pH 3; sweep rate v = 30 mV/s.

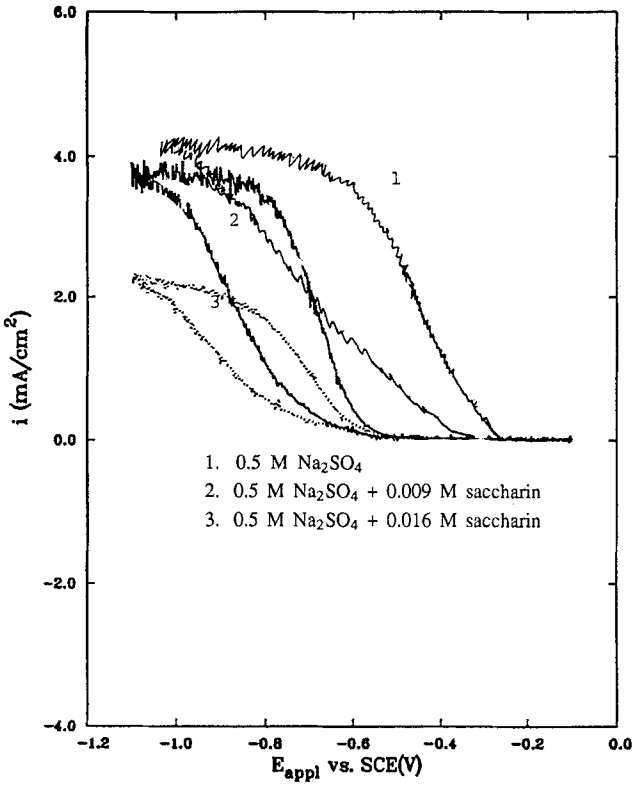

Fig. 3. Effect of saccharin on hydrogen limiting current. Linear sweep voltammetry of Pt rotating disk electrode in 0.5*M* Na_2SO_4; sweep rate = 30 mV/s, pH 3, *w* = 250 rpm.

of 30 mV/s and scanning from −0.1 to −1.4 V *vs.* SCE. The important futures of the results presented in Fig. 4 are the decrease of the hydrogen evolution peak at −0.65 V *vs.* SCE and a cathodic shift of 150 to 200 mV for the hydrogen

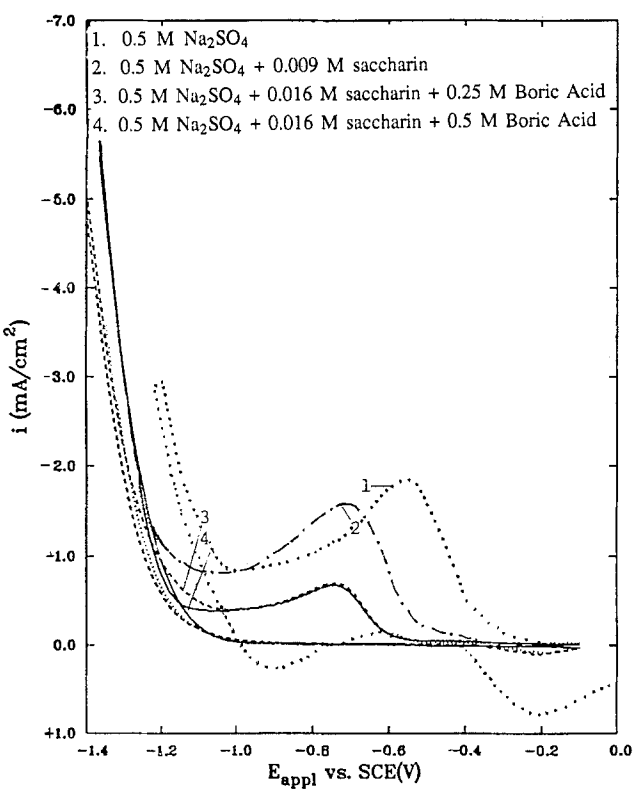

Fig. 4. Effect of saccharin and boric acid on hydrogen evolution. LSV of a Pt rotating disk electrode in 0.5*M* Na_2SO_4, pH 3, sweep rate, *v* = 30 mV/s.

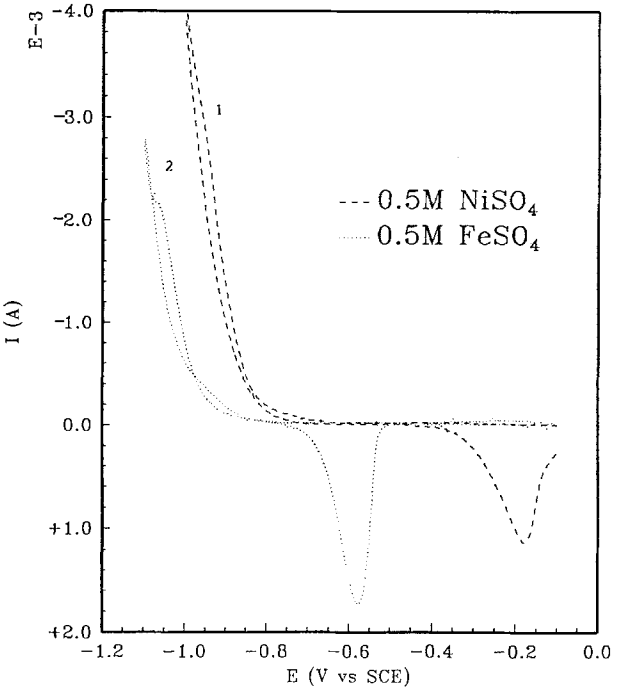

Fig. 5. LSV recorded on copper disk electrodes in electrolyte containing: (1) 0.5*M* $NiSO_4$ + 0.5*M* Na_2SO_4, *v* = 30 mV/s, pH 3; (2) 0.5*M* $FeSO_4$ + 0.5*M* Na_2SO_4, *v* = 30 mV/s, pH 3.

overpotential from water reduction. The maximum decrease in the hydrogen evolution peak at −0.65 V *vs.* SCE and a cathodic shift for the hydrogen overpotential from water reduction of 200 mV occurs when the concentration of saccharin and boric acid in the solution is 0.016 and 0.5*M*, respectively.

By comparing LSVs of pure metal deposition with those when both metals are present in solution one can obtain information about any interaction between the deposition process and deposited metals. The LSVs recorded on a fixed copper disk electrode in electrolyte containing: 0.5*M* $NiSO_4$ + 0.5*M* Na_2SO_4, (curve 1) and in the solution of 0.5*M* $FeSO_4$ + 0.5*M* Na_2SO_4, (curve 2) are shown in Fig. 5. In both cases, one distinct current peak at E_{pa} = −0.19 V (SCE) for dissolution of nickel and at E_{pa} = −0.58 V (SCE) for dissolution of iron appear on the anodic branch of the curve. As shown in Fig. 6, the LSV curve when both metals are present in solution is different to one which would be obtained by superposition of the LSVs pertaining to electrolytes containing pure iron and nickel ions. On the anodic branch of the curve two distinct peaks appear at E_{1pa} = −0.4 V (SCE) and a broad peak at −0.195 V (SCE).

The dissolution peak potential being more positive than that of the pure metal ions may result from a significant change in mixing in the solid phase or formation of intermetallic compounds. Both phenomena may cause the shift of the peak away from its reversible position in the positive direction. The LSV of dissolution of solid solution should possess two separate smooth peaks,[13] the first one corresponding to preferential dissolution of the less noble component at more negative potentials. Since sharp peak occurs at −0.4 V (SCE) in Fig. 6 and taking into account that iron and nickel make intermetallic compounds Fe_3Ni, $FeNi_3$, and FeNi, the peak at −0.4 V (SCE) corresponds to dissolution of Fe from Fe-Ni intermetallic compound, while the peak observed at −0.195 V (SCE) corresponds to apparently passivated nickel stripping peak. The passivation of nickel in the anodic process in sulfate bath has been reported.[14,15] As shown in Fig. 6, I_{pa} at −0.4 V (SCE) increases when higher cathodic overpotentials are applied for the deposition of the alloy indicating that the interaction between the two metals is more pronounced at more negative potentials. A small increase of Ni dissolution peak at E_{pa} = −0.19 V (SCE) also is observed.

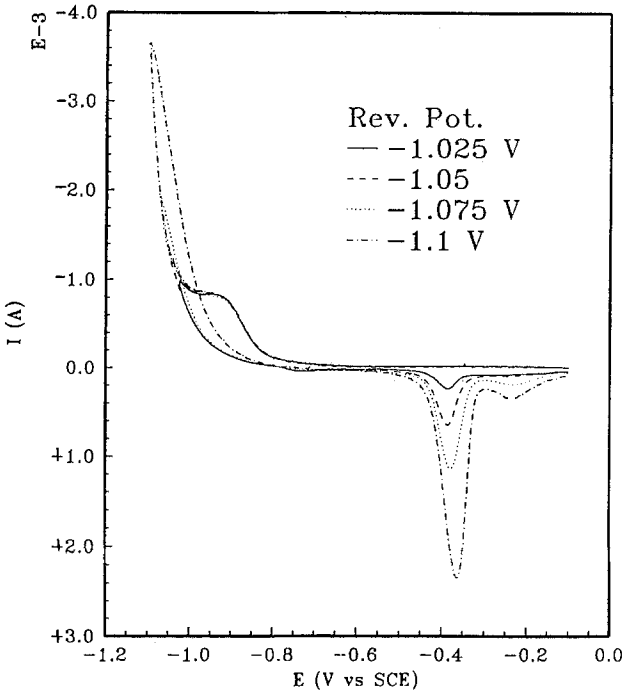

Fig. 6. LSV recorded on fixed copper disk electrode in electrolyte: 0.5*M* $NiSO_4$ + 0.5*M* $FeSO_4$ + 0.5*M* Na_2SO_4 at different reverse potentials; sweep rate, *v* = 30 mV/s, pH 3.0.

In Fig. 7, the LSVs were recorded from electrolytes containing 0.5*M* $NiSO_4$ and 0.2*M* $FeSO_4$, (curve 1) and from the same electrolyte but in the presence of 0.016*M* saccharin, (curve 2). The dissolution of Fe from Fe-Ni intermetallic compound shifts in the cathodic direction. Also, a small increase of the Fe dissolution peak is observed when saccharin is present in the electrolyte.

Galvanostatic pulse and pulse reverse plating.—Galvanostatic pulse and pulse reverse plating of Fe-Ni alloys was carried out in the presence and absence of organic additives. A conceptual diagram of the concentration profiles in the electrolyte is shown in Fig. 8, where $U_{H_2/H^+,ref}$ and $U_{Fe/Fe^{2+},ref}$ are the reference open-circuit potentials for the hydrogen and iron reactions, respectively. The reference state is set as the bulk equilibrium condition for convenience.[16] The nickel reaction is not shown because of its minor role. The potential rises during T_{on} because concentration depletion becomes more severe with time. It is assumed and also is evident from the experiments that the pr mode yields less cathodic E_p during the pulse period but more anodic E_r during the relaxation period compared to the pc mode under the same i_p.

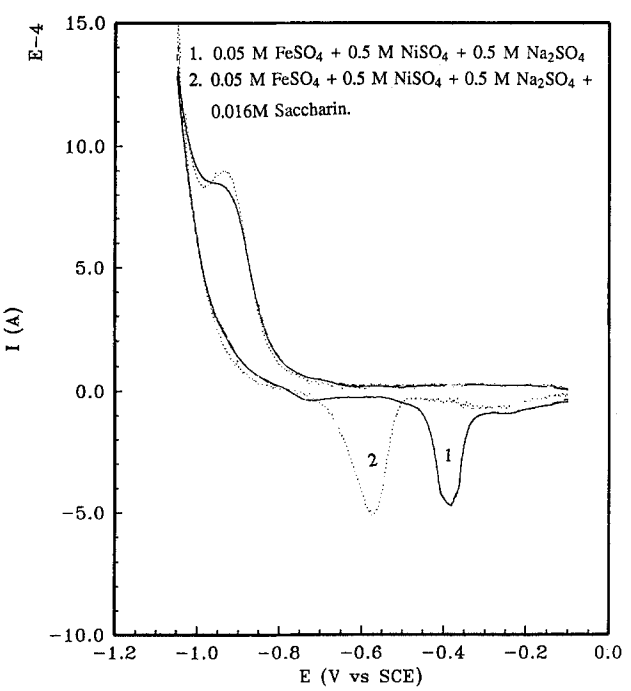

Fig. 7. LSV recorded on copper disk electrodes in electrolyte containing: curve (1) 0.05*M* $FeSO_4$ + 0.5*M* $NiSO_4$, pH 3, reverse potential E_r = −1.05 V (SCE), sweep rate, *v* = 30 mV/s; curve (2) 0.05*M* $FeSO_4$ + 0.5*M* $NiSO_4$ + 0.016*M* saccharin, pH 3.0, reverse potential, E_r = −1.05 V (SCE), *v* = 30 mV/s.

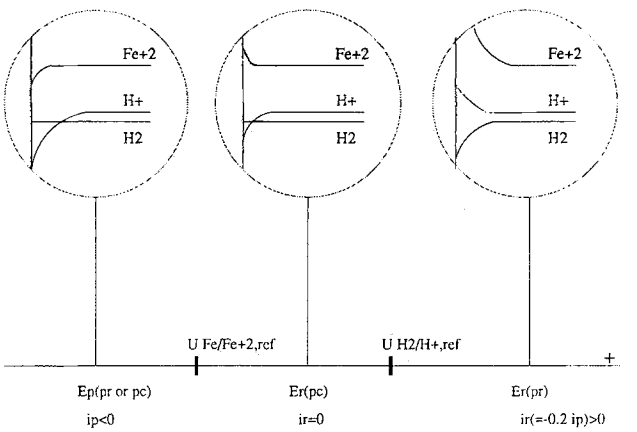

Fig. 8. A schematic diagram of concentration behavior at different stages for pr or pc. [For reference: $a_{H^+,bulk}$ = 1 × 10^3*M*, $C_{Fe^{+2},bulk}$ = 0.05*M*, $C_{H_2sat.}$ = 7.816 × 10^{-4}*M* at 298 K. (In a system with significant hydrogen evolution, $C_{H_2sat.}$ can be taken as a lower bound if supersaturation of H_2 occurs.)]

The smaller amount of replenishment of reactant during T_{off} for the pc mode induces more cathodic potential during T_{on}, while the applied anodic current during T_{off} for the pr mode forces more anodic potential as compared to that of the pc mode. In the pc mode, *E* is the mixed potential between the open-circuit potential of Fe/Fe^{+2} and H_2/H^+ so that the net current is zero.[17] The reduction of H^+ occurs not only during T_{on} but also during T_{off}. At the onset of T_{off}, the severe H^+ depletion at the end of T_{on} causes a more cathodic potential to favor the reduction of H^+. As time proceeds the supply of H^+ from the bulk solution causes the mixed potential to move toward more anodic potentials. A schematic explanation of this phenomenon is shown in Fig. 9a. For the pr mode, both H_2 and Fe oxidize during T_{off}. As one can see from Fig. 9b, the reaction 1/2 H_2 = H^+ + *e* is favored at the

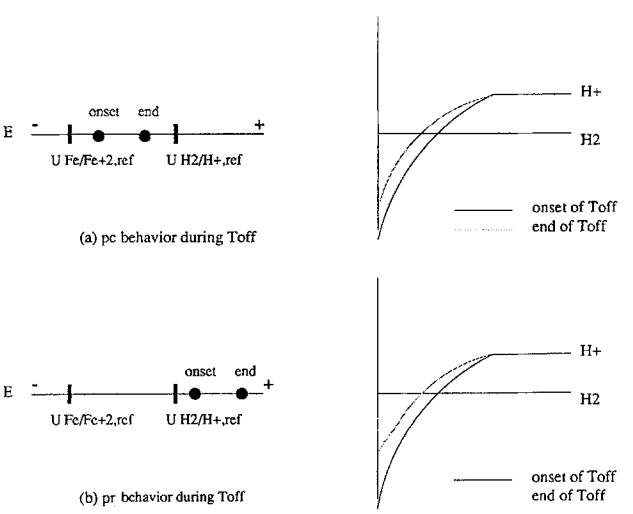

Fig. 9. (a) Schematic potential responses and associated H^+ behavior in pc mode during T_{off}; (b) schematic potential responses and associated H^+ behavior in pr mode during T_{off}.

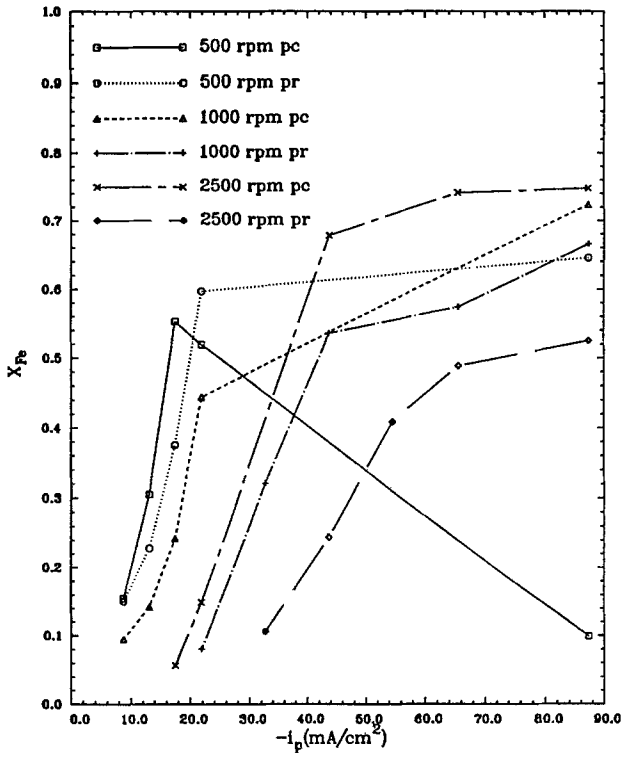

Fig. 10. Iron composition profiles as a function of pulse peak current at various rotation speeds for pc and pr mode.

beginning of T_{off}, where H^+ depletion is most severe. As time proceeds, the supply of H^+ from the bulk and the depletion of H_2 at the interface force a more anodic potential as shown schematically in Fig. 9b. The argument that applies to H_2/H^+ can be applied to Fe/ Fe^{+2} as well.

Figure 10 shows the iron composition X_{Fe} *vs.* i_p in both pc and pr modes. In the low i_p region, X_{Fe} increases rapidly with i_p, and levels off at higher i_p (with the exception of pc curve at 500 rpm, which is discussed later). At low i_p, Fe deposition is totally under kinetic control and an increase of the cathodic polarization enhances the Fe deposition rate significantly. However, the limitation of mass transfer becomes more important at higher i_p, causing a flattening of Fe content in Fig. 10. The significant drop of X_{Fe} at low rotation speeds and higher i_p is due to the influence of solution chemistry at the electrode interface.[6,10] Due to the much lower stability constant of $Ni(OH)_2$ relative to that of iron hydroxide, more $Ni(OH)_2$ precipitates on the electrode at lower rotation speeds and at high applied current densities, where the proton depletion is most significant. For comparison, in the pr mode such precipitation at high interfacial pH is less evident because the replenishing of H^+ by reaction $1/2\ H_2 = H^+ + e^-$ occurs during T_{off} period.[11]

For the pc mode at low i_p, (*e.g.*, less than 15 mA/cm^2) the iron content decreases as the rotation speed increases. In this region the main electrode reactions may be hydrogen evolution and nickel deposition. An increase of the rotation speed enhances the mass transfer which favors the hydrogen discharge. However, at higher i_p, the Fe^{2+} reduction rate becomes significant because E_p is raised to a sufficiently negative potential at which the mass-transfer limitation is the major factor affecting the iron content. As a consequence, higher rotation corresponds to larger X_{Fe}. According to Fig. 10, the same electrode rotations, X_{Fe} is always lower for pr compared with the X_{Fe} values obtained in pc mode, except for a special case (*i.e.*, low rpm, high i_p in pc mode). It is natural to conclude that dissolving Fe by the anodic current (i_r) during T_{off} causes less Fe content in the case of pr than in pc mode. As mentioned earlier, the dissolution of the alloy affects the Fe dissolution more than Ni dissolution, because Ni is passivated during the anodic process in a sulfate bath. During T_{off} in the pc mode, Fe is forced to dissolve at the same rate as the hydrogen discharge reaction to maintain a zero net current. Thus, the mixed electrode potential is between the open-circuit potential of H_2/H^+ and Fe/Fe^{2+}. However, such dissolution of Fe is insignificant compared to the externally forced dissolution in pr mode.

For the pr mode, a higher rotation speed consistently reduces the iron content in the whole i_p range. The explanation of this phenomena is given in Fig. 11a. Since Ni is passivated during the anodic process, only Fe and H_2 participate in the oxidation process during T_{off} period. At high rotation speeds, one expects proton depletion to be less severe at the end of T_{on}. As a consequence, oxidation of H_2 is at a lower rate during T_{off} because of a higher product concentration (H^+) at the end of T_{on}. Thus, for a given i_r, more anodic potentials favor the Fe dissolution which reduces the Fe content in the deposit.

The effect of rotation speed on pc and pr modes is totally opposite for high i_p regions, suggesting that the influence of enhanced convection can be completely diverse depending on whether the mode is with or without reverse current.

Figure 12 shows the effect of the additives on alloy composition. The influence of additives can be viewed as a surface-coverage mechanism. The fractional coverage of the electrode surface by an additive allows the electrode to be polarized much more in either cathodic or anodic direction without causing reactant concentration depletion at a specific applied current density. The concentration overvoltage is reduced and the surface overpotential is increased due to the less effective exchange current density

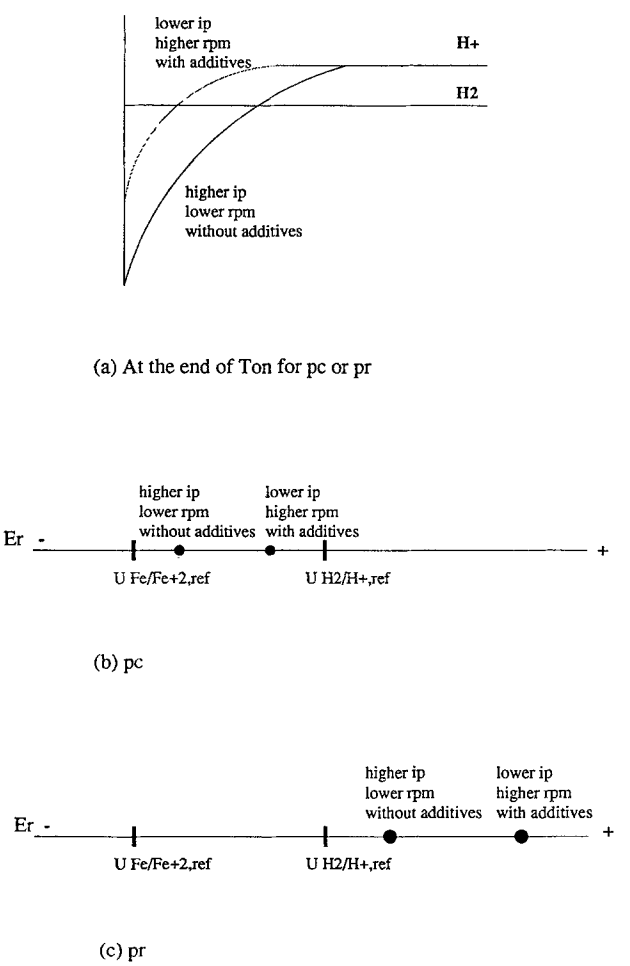

Fig. 11. (a) Effect of pulse current density, rotation speed, and effect of the additives on the H^+ concentration profile at the end of T_{on}. (b) Effect of pulse current density, rotation speed, and effect of the additives on E_r for pc mode. (c) Effect of pulse current density, rotation speed, and effect of the additives on E_r for pr mode.

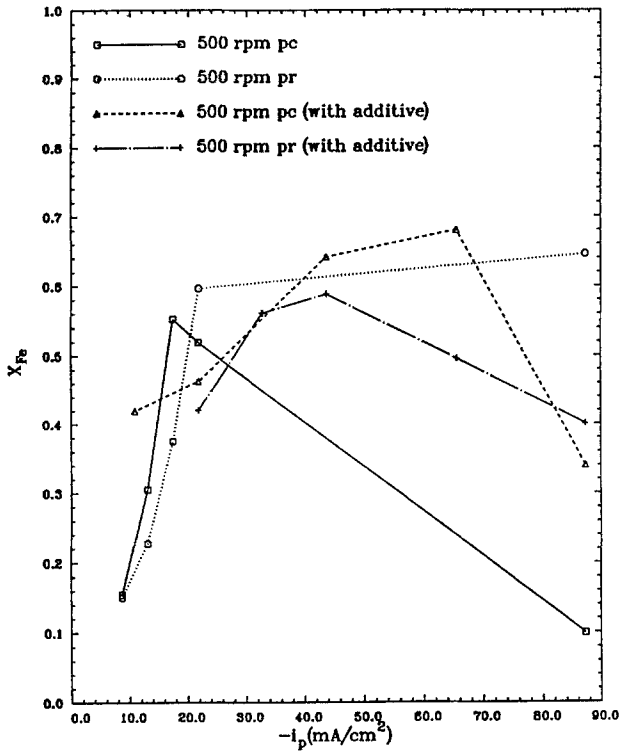

Fig. 12. Additive effect on the alloy composition.

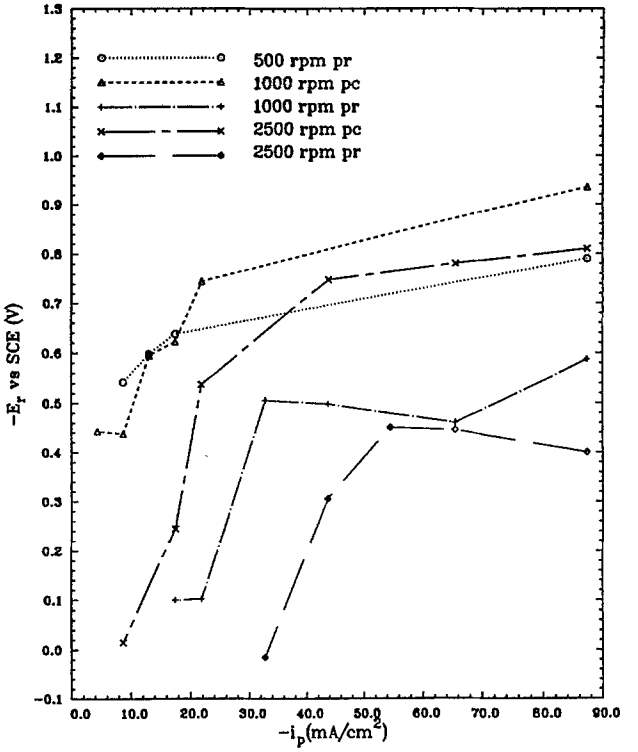

Fig. 14. Potential response during T_{off}.

causing the operating potential range to be more extended. According to the results obtained in this study (Fig. 1-3), by adding organic compounds, the proton concentration depletion significantly decreases causing $Ni(OH)_2$ precipitation to be eliminated at higher i_p. As seen in Fig. 12, the humps of the X_{Fe} profile shift to a more cathodic current density and become broader, suggesting that the influence of mass-transfer limitation on Fe deposition is delayed.

For the pr mode, introducing additives in the electrolyte reduces the iron content in the deposit. A qualitative explanation of this phenomena is shown in Fig. 11b. In the presence of additives in the electrolyte, the proton concentration is less depleted during T_{on} period as a result of the surface-coverage effect. As a consequence, during T_{off} period the rate of hydrogen oxidation decreases due to the smaller area available for oxidation and because of the higher proton concentration. Thus, more anodic potential is anticipated in the presence of organic compounds for a given applied i_p than in the absence of the additives, which favors the dissolution of Fe. This is a qualitative argument; to quantify the effect, a detailed mathematical model must be developed.

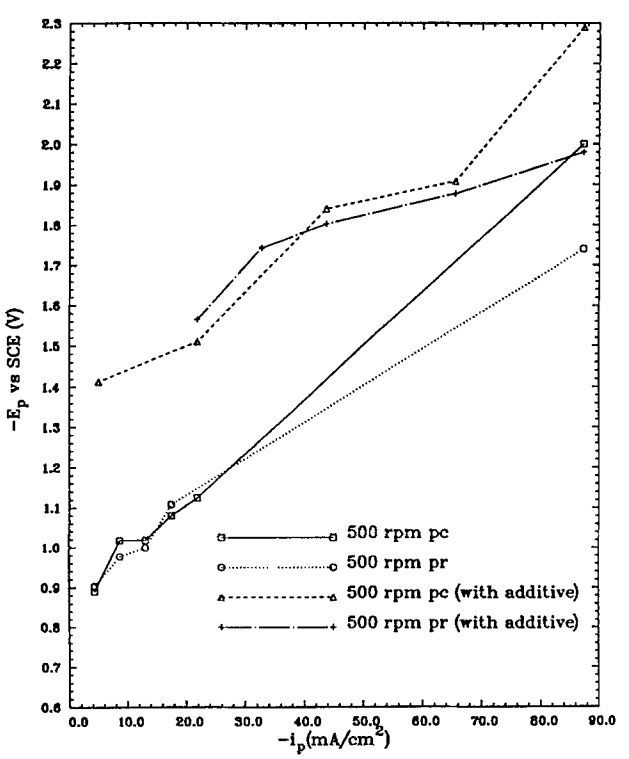

Fig. 13. Additive effect on the potential responses during T_{on}.

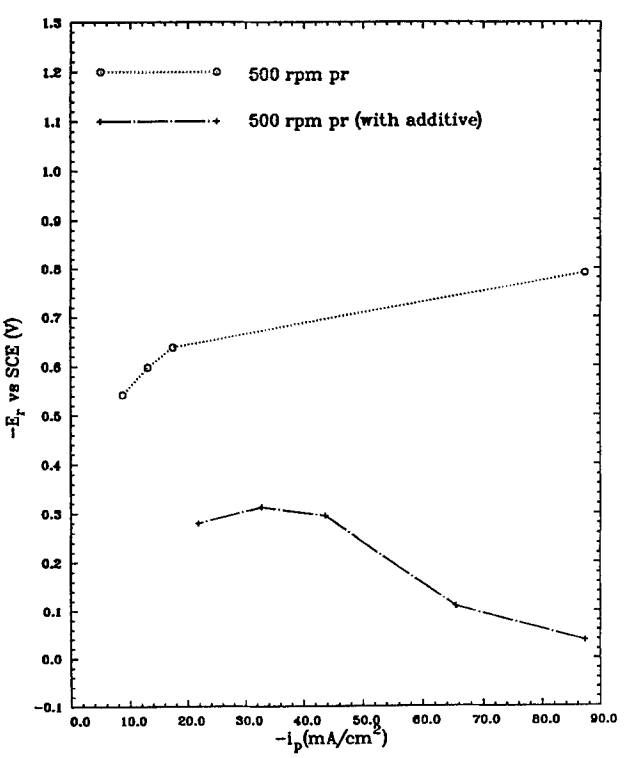

Fig. 15. Additive effect on the potential responses during T_{off}.

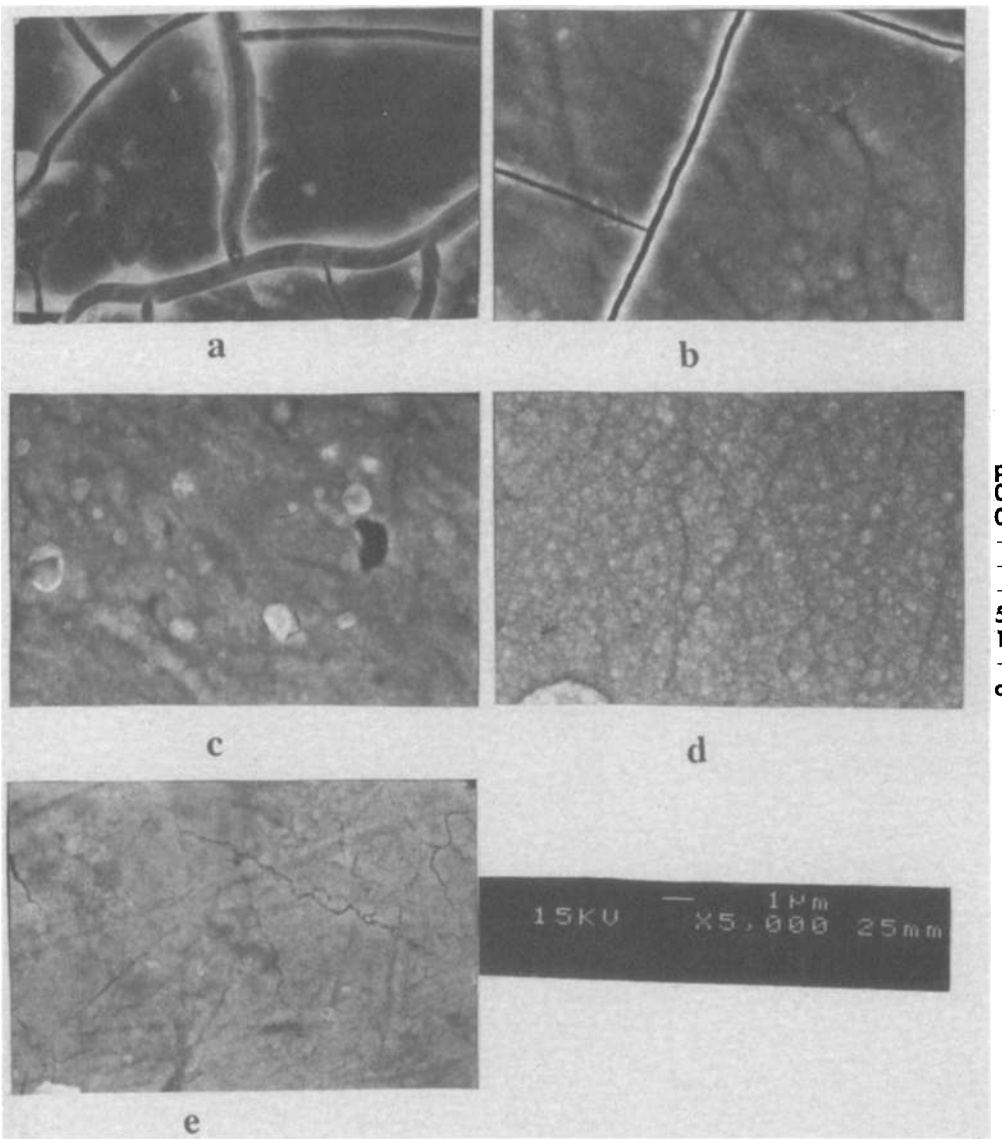

Fig. 16. SEMs of an alloy deposited from a bath containing: 0.5M $NiSO_4$ + 0.05M $FeSO_4$ + 0.5M Na_2SO_4, pH 3; and (a) i = −87.3 mA/cm^2, 500 rpm; (b) i_p = −21.8 mA/cm^2, 500 rpm; (c) i_p = −21.8 mA/cm^2, i_r = 4.4 mA/cm^2, 500 rpm; (d) i_p = −21.8 mA/cm^2, 1000 rpm; and (e) i_p = −65.5 mA/cm^2, i_r = 13.1 mA/cm^2, 1000 rpm.

The pulse potential responses in Fig. 13 indicate that the pc mode induces more cathodic potential than the pr mode except in the low i_p region where the difference between these two is not significant. In the pc mode higher proton concentration and Fe^{2+} depletion is observed during T_{on} period since less replenishing of these reactants occurs during T_{off} as compared to the pr mode, where enforced dissolution of Fe is present in the relaxation period. Also, the enhanced polarization caused by the presence of organic additives is more pronounced in the case of pc compared to the pr mode. As explained earlier, the increased polarization is caused by the less available reactive area due to the additive coverage. A theoretical potentiostatic model including the additive effect explains the enhanced polarization well.[18] The positive role of the surface agents is that the potential drop in their presence in the electrolyte is absorbed by the slower kinetics than by the large concentration overpotential.

T_{off} potential responses under various operating conditions are given in Fig. 14. As seen from this figure, E_r shifts in cathodic direction as i_p (also i_r) increases in both modes. Figure 9a-b illustrate the relationship of E_r with i_p for pc mode. At higher i_p, the pH is higher at the interface at the end of T_{on}. During T_{off}, the mixed potential moves to a more cathodic position to favor proton reduction (Fig. 9b). The rate of iron oxidation probably is less affected by changing i_p because the reduction product is on the solid phase.

More cathodic E_r as i_p increases was observed also in the pr mode. One expects E_r to become more anodic as i_p increases in this mode since larger $i_r = 0.2i_p$ is applied during T_{off}. The observed behavior is again explained by the H^+ depletion during T_{on} (Fig. 9a). A higher i_p induces lower H^+ at the interface during the cathodic process which gives a larger driving force for the oxidation of H_2 during T_{off}. Thus, less anodic E_r as it is seen in Fig. 9c is expected. Higher i_p means higher i_r which causes the potential to be more anodic. The effect of H^+ depletion during T_{on} period counteracts with the enforced i_r during T_{off} and controls the shape of E_r curves in pr mode. In Fig. 14, the competition of these two factors is manifested by the flattening of E_r at higher i_p values.

Enhanced convection seems to force both pr and pc E_r curves to a more anodic direction, which is consistent with the H^+ depletion argument (Fig. 9a). Higher rotation speeds induce less depletion during T_{on} which gives less driving force for the oxidation of H_2 during T_{off} but higher driving force for the reduction of H^+. As a consequence, more anodic E_r is required to maintain a forced i_r in pr mode (Fig. 9b).

Figure 15 shows the effect of the organic additives on E_r. A significant anodic shift of E_r in the pr mode is observed when the experiments were carried out with electrolytes which contain organic additives. Addition of organic surfactants reduce the proton concentration depletion during T_{on} period, and does not give sufficient driving force for hydrogen oxidation during T_{off} period thereby causing more anodic E_r compared with the bath without additives. In addition, the reduction of the reactive surface area con-

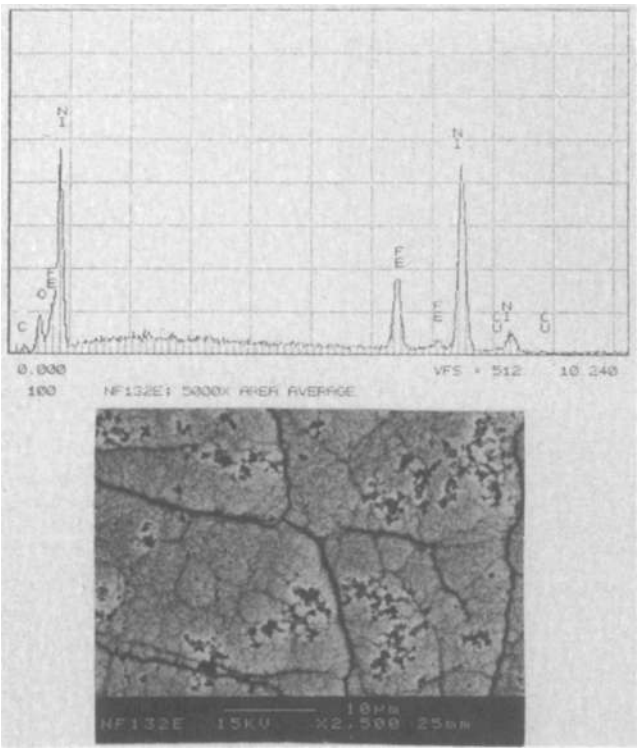

Fig. 17. SEM and EDS spectra taken at the edge of the plate deposited from a bath containing: 0.005*M* $FeSO_4$ + 0.5*M* $NiSO_4$ + 0.5*M* Na_2SO_4, pH 3.

tributes the potential to shift more in the anodic direction during T_{off} period. From Fig. 15, another interesting phenomena is observed; E_r becomes more anodic as i_p increases. Less available active surface area causes E_r to be more anodic when $i_r = 0.2i_p$ increases. Roha and Landau[19] in their modeling paper have shown that surface coverage increases with applied current when the deposition process is carried out in the presence of organic additives. Their model is consistent with our experimental results that large surface coverage is expected at higher i_p causing more anodic E_r to maintain i_r during T_{off}. The above discussion indicates the importance of additives in affecting the mechanism of the pulse alloy plating.

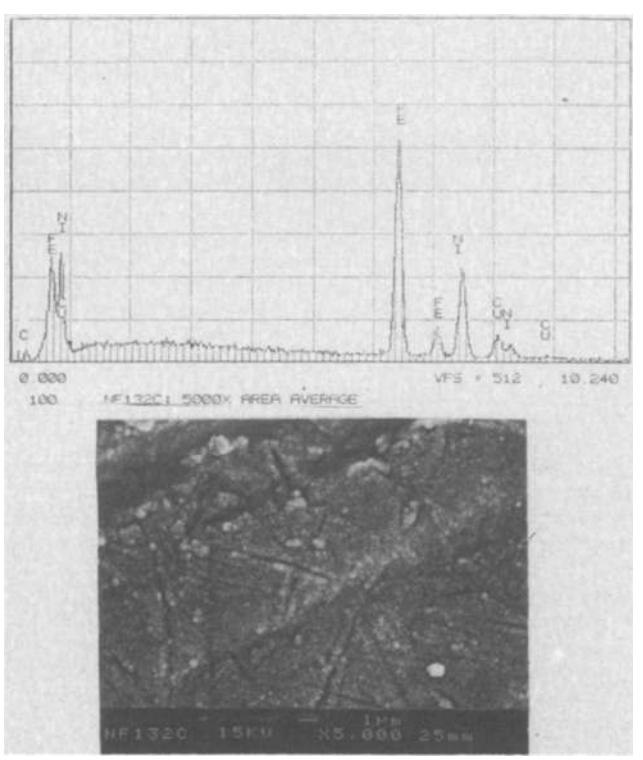

Fig. 18. SEM and EDS spectra taken at the center of the plate deposited from a bath containing 0.005*M* $FeSO_4$ + 0.5*M* $NiSO_4$ + 0.5*M* Na_2SO_4, pH 3.

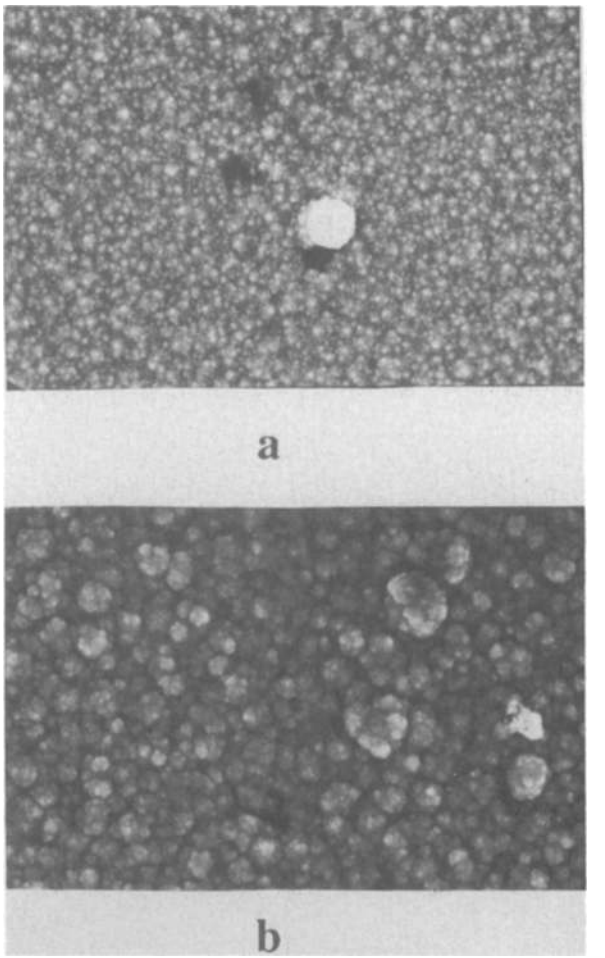

Fig. 19. SEMs of an alloy deposited from a bath containing: 0.005*M* $FeSO_4$ + 0.5*M* $NiSO_4$ + 0.5*M* Na_2SO_4, pH 3; (a) using galvanostatic pulse technique, $i_p = -65$ mA/cm^2 at $w = 2500$ rpm; and (b) using galvanostatic pulse reverse technique, $i_p = -65.5$ mA/cm^2, $i_r = 13.1$ mA/cm^2 at $w = 2500$ rpm.

Morphology of the coatings.—To study the influence of the organic additives and the rotation speed of the electrode on the morphology of the electrodeposited Fe-Ni alloy, investigations were carried out using SEM. Typical SEM micrographs of the deposits prepared by both modes are shown in Fig. 16. For the pc mode (Fig. 16a-b) under low rotation speeds and high i_p, the deposits are cracked. The SEMs at the black edges show a porous structure. The higher current density on the edge results in a high hydrogen evolution reaction rate. As a consequence higher rise of pH at the edges occurs which induces a porous precipitation of $Ni(OH)_2$, or $Fe(OH)_2$. Figure 17-18 represents a comparison of EDS spectrum obtained at the edge and at the center of the plates deposited at high peak currents (87.3 mA/cm^2 under stationary conditions and at the pc mode). A clear oxygen peak occurring simultaneously with the nickel peaks at the edges indicates the existence of $Ni(OH)_2$ rather than $Fe(OH)_2$. Thus, more $Ni(OH)_2$ precipitates on the electrode at higher peak currents under stationary conditions (or at lower rotation speeds). An average of 0.2 to 0.3 of Fe mole fraction was observed at the edges of the electrode compared with values of 0.4 to 0.6 mole fractions of Fe observed at the center of the plate in

agreement with the results obtained by plating Fe-Ni under potentiostatic conditions.[21] These results are not consistent with Dahms and Croll's theory.[1] Dahms and Croll suggested that the preferential adsorption of $Fe(OH)_2$ rather than $Ni(OH)_2$ on the electrode at high pH values. The adsorbed $Fe(OH)_2$ inhibits the discharge rate of nickel but does not interfere with iron deposition. However, according to the solution chemistry as shown in Ref. 6 and 21, $Ni(OH)_2$ should be precipitated preferentially rather than $Fe(OH)_2$. Because of the difference in metal hydroxide ion stability constants (K_{sp} of $Ni(OH)_2 = 6.3 \times 10^{16}$ mol/liter, K_{sp} of $Fe(OH_2)$ mol/liter), $Ni(OH)_2$ precipitation occurs at a pH smaller by two units than $Fe(OH)_2$ precipitation. To support the preferential adsorption of $Fe(OH)_2$, we must assume that both $Fe(OH)_2$ and $Ni(OH)_2$ are in the form of colloids and have different adsorption rates which is not reasonable. Cracking is caused by the relaxation of metal hydrides which are formed along the hydrogen evolution reaction.[22] By reducing i_p, using the pr mode as a deposition technique, by increasing rotation speed and by adding organic additives in the plating solution one can reduce the chance to plate Fe-Ni cracked deposits. The leveling effect is evident for the deposits plated from the baths which contain organic additives. According to Fig. 19a and b, the deposit grain size increases when using pulse reverse mode as a plating technique. The crystal growth rate is proportional to the surface adatom concentrations surrounding the site. Taking into account that the surface adatom concentration is proportional to the solution concentration in the vicinity of the electrode one can expect that pulse reverse mode has a higher growth rate compared with pc mode under the same diffusion coefficient. Also, pr induces less cathodic potential than pc mode does. According to Puippe,[18] the nucleation rate is enhanced by increasing the overpotentials. The pulse reverse mode has an ability to induce less nucleation rate than pc and it is expected to deposit larger grain size since the deposit grain size is proportional to the crystal growth rate and inversely proportional to the nucleation rate.

As seen in Fig. 20a and b, the leveling effect is evident for the deposits plated from the baths which contain organic additives. Best alloy appearance was observed when the electrodeposition was carried out using pulse reversal technique with $i_p = 65$ mA/cm^2 and $i_r = 13.1$ mA/cm^2 at rotation speed from 500 to 2000 rpm and using electrolyte containing: 0.5*M* $NiSO_4$ + 0.05*M* $FeSO_4$ + 0.5*M* boric acid + 0.016*M* saccharin and 0.116*M* 2-butene, 1-4 diol and for longer deposition time.

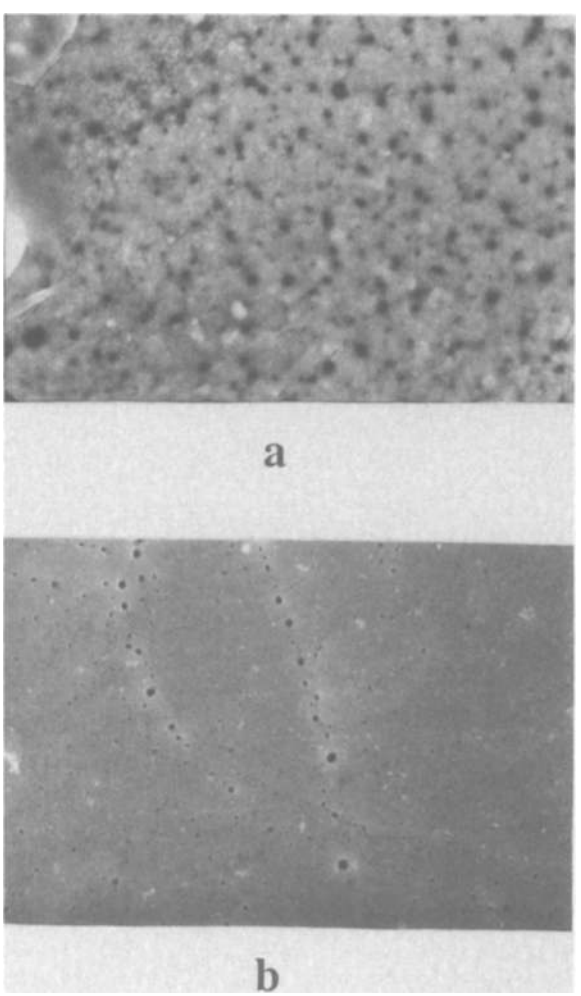

Fig. 20. SEM spectrum of an alloy deposited using pulse reverse technique from a bath containing: 0.005*M* $FeSO_4$ + 0.5*M* $NiSO_4$ + Na_2SO_4, pH 3, w = 500 rpm; (a) in the presence of 0.009*M* saccharin; (b) in the presence of 0.016*M* saccharin + 0.116*M* 2-butene, 1-4 diol + 0.5*M* boric acid.

Conclusion

The influences of i_p, i_r, electrode rotation speed and the presence of organic additives in the bath on galvanostatic pulse and pulse reverse Fe-Ni plating were studied using rotating disk electrodes in sulfate baths. When low peak potentials are applied in pc or pr mode, iron content in the deposit increases rapidly with the increase of the peak potential and levels off at higher peak potentials. At low i_p, iron deposition is under kinetic control and an increase of the cathodic polarization enhances iron deposition rate. Limitation of mass transfer becomes more important at higher i_p, causing a flattening of X_{Fe} *vs.* i_p curve. The significant drop of x_{Fe} at low rotation speed and higher i_p is due to the much lower stability constant of $Ni(OH)_2$ relative to that of iron hydroxide. More $Ni(OH)_2$ precipitates on the electrode at lower rotation speeds and at higher applied current densities, where the proton depletion is most significant.

For the pc mode and at low i_p, the iron content decreases as the rotation speed increases. In this region the main electrode reactions are hydrogen evolution and nickel deposition. An increase of the rotation speed enhances the mass transfer which favors the hydrogen discharge. At higher i_p, the Fe^{2+} reduction rate becomes significant because E_p is raised to a negative enough potential at which the mass-transfer limitation is the major factor affecting the iron content. Thus, at this region, higher electrode rotation speed corresponds to larger X_{Fe}.

For the pr mode, a higher rotation speed consistently reduces the iron content in the whole i_p range. In this mode for a given i_p, more anodic potentials (present at this mode) favor the Fe dissolution, which reduces the Fe content in the deposit.

In the presence of organic additives, the fractional coverage of the electrode surface allows the electrode to be polarized more in either cathodic or anodic direction without causing reactant concentration depletion at a specific applied current density. The proton concentration depletion significantly decreases causing $Ni(OH)_2$ precipitation to be eliminated at higher i_p. For the pr mode, with introducing organic additives in the electrolyte more anodic potential is anticipated for a given i_p which favors the dissolution of Fe from the alloy. The pc mode induces more cathodic potential than the pr mode except in the low i_p region where the difference between these two is not significant. Enhanced convection seems to force both pr and pc E_r curves to a more anodic direction, which is consistent with the H^+ depletion argument. Higher rotation speeds induce less depletion during T_{on} which gives less driving force for the oxidation of H_2 during T_{off} but higher driving force for the reduction of H^+. Addition of organic surfactants reduces the proton concentration depletion during T_{on} period in pr mode and does not give sufficient driving force for hydrogen oxidation during T_{off} period; thus causing more anodic E_r compared with the bath without additives. Since pr mode induces less cathodic potential than pc mode does, and since the nucleation rate is enhanced by increasing the overpo-

tentials, pulse reverse mode in the case of Fe-Ni plating has an ability to induce less nucleation rate than pc and to deposit Fe-Ni layers with larger grain size.

Acknowledgment

This work was supported by Sandia National Laboratories and AESF project RF-83.

Manuscript submitted Sept. 10, 1992; revised manuscript received Jan. 11, 1993.

The University of South Carolina assisted in meeting the publication costs of this article.

REFERENCES

1. H. Dahms, *J. Electroanal. Chem. Interfacial Electrochem.*, **8,** 5 (1964).
2. H. Dahms and I. M. Croll, *This Journal,* **112,** 771 (1965).
3. P. C. Andricacos, C. Arana, J. Tabib, J. Dukovic, and L. T. Romankiw, *ibid.,* **136,** 1336 (1989).
4. P. C. Andricacos, J. Tabib, and L. T. Romankiw, *ibid.,* **135,** 1172 (1988).
5. B. N. Popov, K. Ming Yin, and R. E. White, *AESF SUR/FIN '92, International Technical Conference Proceedings,* p. 53 (1992).
6. K. Ming Yin, B. N. Popov, and R. E. White, *ibid.,* p. 103 (1992).
7. L. T. Romankiw, in *Proceedings of the Symposium on Electrodeposition Technology, Theory and Practice,* L. T. Romankiw, Editor, PV 87-17, p. 301, The Electrochemical Society Proceedings Series, Pennington, NJ (1987).
8. M. J. Nichol and H. I. Philip, *Electroanal. Chem. Interfacial Electrochem.,* **70,** 233 (1976).
9. S. Swathirajan, *This Journal,* **133,** 671 (1986).
10. S. Hessami and C. W. Tobias, *ibid.,* **136,** 3611 (1989).
11. D. L. Grimmett, M. Schwartz, and K. Nobe, *ibid.,* **137,** 3414 (1990).
12. B. V. Tilak, A. S. Gendron, and M. A. Mosoin, *J. Appl. Electrochem.,* **7,** 495 (1977).
13. S. Swathirijan, *This Journal,* **133,** 671 (1986).
14. D. Jovic, R. M. Zejnilovic, A. R. Despic, and J. S. Stevanovic, *J. Appl. Electrochem.,* **18,** 511 (1988).
15. J. H. Gerretsen and J. H. DeWit, *ibid.,* **21,** 276 (1991).
16. R. E. White and S. E. Lorimer, *This Journal,* **130,** 1096 (1983).
17. K. Ming Yin and R. E. White, *AIChE J.,* **36,** 187 (1990).
18. J. C. Puippe, *Theory and Practice of Pulse Plating,* J. C. Puippe and F. Leaman, Editors, p. 17, American Electroplaters and Surface Finishers Society, Orlando, FL (1986).
19. D. Roha and U. Landau, *This Journal,* **137,** 824 (1990).
20. B. N. Popov, Ken Ming Yin, and R. E. White, Submitted for publication to the Technical Editor of the *Plating and Surface Finishing* (1992).
21. K. Ming Yin, B. N. Popov, and R. E. White, *ibid.,* Submitted.
22. N. Hackerman and T. Jensen, *This Journal,* **99,** 60 (1952).

Conductivities and Densities of Na_2SO_4-$NaVO_3$ Melts

Xuejin Zheng, Robert A. Rapp,* and Kazuhiro Goto[a]

Department of Materials Science and Engineering, The Ohio State University, Columbus, Ohio 43210

ABSTRACT

Electrical conductivities and densities of Na_2SO_4-$NaVO_3$ (0-30 m/o $NaVO_3$) melts have been measured in a temperature range of 1150 to 1220 K by an electrochemical impedance technique and by an Archimedean method. The specific conductivities of the melts decrease with increasing amount of $NaVO_3$ in the melts, which results from a decrease in the Na^+ densities. As temperature increases, the specific conductivities of the melts increase. The densities of the melts increase both with increasing amount of $NaVO_3$ in the melts and with decreasing temperature. From the specific conductivities and densities of the melts, the equivalent conductivities and the Na^+ densities of the melts were calculated.

Electrical conductivity is an important property of an electrolyte, and fused salts are known to be electrolytes with high conductivities. The conductivity of an electrolyte can be expressed as its specific conductivity or equivalent conductivity. To obtain an equivalent conductivity, the density of the electrolyte is required. The electrochemical impedance technique was used here to measure the specific conductivities of Na_2SO_4-$NaVO_3$ [0-30 mole percent (m/o) $NaVO_3$] melts in a temperature range of 1150 to 1220 K. The densities of the melts were measured by the Archimedean method to permit calculation of the equivalent conductivities and the Na^+ densities of the melts. Vanadium exists as multivalence ions. Mittelstadt and Schwerdtfeger[1] studied the oxidation states of vanadium in $NaVO_x$ melts by thermogravimetric analysis. In analog to iron-containing slags with both ferric and ferrous ions,[2] one might suppose that electron hopping could occur between vanadium ions of different valence, which would contribute to the conductivity of the fused salt. Our purpose was to ascertain whether partial electronic conduction contributes significantly to the electrical conductivity of the melts.

Experimental Procedure

The experimental apparatus used for the conductivity measurements in this study is illustrated in Fig. 1. A two-electrode system was used with a main conduction path limited to the salt within a pair of alumina capillaries of about 2 mm id and 30 mm long, to provide a cell constant of approximately 190 cm^{-1}. An alumina crucible was used to contain the melt. The cell constant was calibrated at room temperature using a 0.1*N* KCl aqueous solution which has a well-known conductivity.

A one-end-closed mullite tube of 54 mm id containing the experimental cell was closed by a gas-tight, water-cooled stainless steel flange sealed by Ceramabond. Several adapters and holes in the top flange allowed the electrodes and conduit tubes to be inserted into the reaction chamber which was positioned in a vertical tubular electric furnace. The temperature was controlled within ±2 K by a solid-state temperature controller (Barber-Colman 520) using a type-S (Pt-Pt/10%Rh) thermocouple which was located near the heating element of the furnace. Another type-S thermocouple positioned in the reaction chamber near the fused salt melt was used to measure the experimental temperature.

* Electrochemical Society Active Member.
[a] Present address: University of Rio Grande Japan, Tanashi City, Tokyo 188, Japan.